Supporting Information for

Dependence of Copper(I) Stability on Long-range Electromagnetic Effects of Au under Reducing Atmospheres: the Size Effect of Au Cores

Xin Huang,[a,b] Haitao Li,[*a] Bin Zhang,[c] Yin Zhang,[a] Hao Wang,[a] Lijun Ban,[a] Yixuan Xu,[a] Yongxiang Zhao[*a]

[a] Engineering Research Center of Ministry of Education for Fine Chemicals, School of Chemistry and Chemical Engineering, Shanxi University, Taiyuan 030006, China.

[b] Department of Chemistry and Chemical Engineering, Jinzhong university, Jinzhong 030619, China.

[c] State Key Laboratory of Coal Conversion, Institute of Coal Chemistry, Chinese Academy of Sciences, Taiyuan 030001, China.

*CORRESPONDING AUTHORS

Address: Shanxi University, 92 Wucheng Road ,Taiyuan 030006, China.

Haitao Li, Email: htli@sxu.edu.cn

Yongxiang Zhao, Email:yxzhao@sxu.edu.cn

1. CHARACTERIZATIONS

The amounts of Cu and Au in the catalysts were determined using an iCAP 7400 ICP-OES inductively coupled plasma emission spectrometer (Thermo Fisher Scientific, USA).

Transmission electron microscopy (TEM), high-resolution transmission electron microscopy (HR-TEM), and high angle annular dark-field scanning transmission electron microscopy (HAADF-STEM) analyses were performed using a USA FEI TECNAI G2 F20 S-TWIN TEM, operated at 200 kV. Energy-dispersive X-ray spectroscopy (EDS) experiments were performed using an Oxford EDAX Genesis transmission electron microscope.

X-ray diffraction (XRD) patterns were recorded on a Bruker D8 Advance X-ray diffractometer with Cu Kα rays (λ = 1.542 Å) at a voltage of 40 kV, current of 40 mA, and a scanning speed of $0.1°·s^{-1}$, where the size of metal oxide was obtained by the Scherrer equation $D = K\lambda/(\beta\cos\theta)$.

The H_2-TPR test was performed on a USA Micromeritics AutoChem II 2920 fully automated programmable temperature chemisorption instrument with a catalyst loading of 30 mg. The sample was purged with Ar for 30 min at 200 °C, cooled to room temperature, purged with a 5%/95% mixture of H_2/Ar at a flow rate of 40 ml/min and a heating rate of 10°C/min, and the hydrogen consumption was detected by TCD.

X-ray photoelectron spectroscopy (XPS) and X-ray Auger electron spectroscopy (XAES) measurements were performed on an Thermo SCIENTIFIC K-Alpha(Thermo Fisher Scientific, USA) using a monochromatic Al Kα-ray source (hν = 1486.8 eV), and the binding energy in the spectrum was calibrated from contaminant carbon (*C 1s* = 284.8 eV).

The ultraviolet photoelectron spectra (UPS) were acquired on a commercial "Thermo Scientific K-Alpha" using 21.2 eV of Helium discharge as the excitation source, and a negative

bias of −5 V was applied during the measurement. Charge correction was carried out using the binding energy standard of **C1s**=284.8 eV.

Raman spectra were obtained from a LabRAM HR Evolution Raman spectrometer (HORIBA Scientific, France), the laser was focused on the sample surface through a 50×long-distance objective lens with a 1 μm spot size. A holographic grating of 1800gr/mm was used, and the acquisition time was 10 s. The Raman spectra were obtained with an acquisition time of 10 s and collection number of 1, using a holographic grating with 1800 grooves/mm. The Raman band of the silicon wafer at 520.7 cm^{-1} was employed to calibrate the spectrometer.
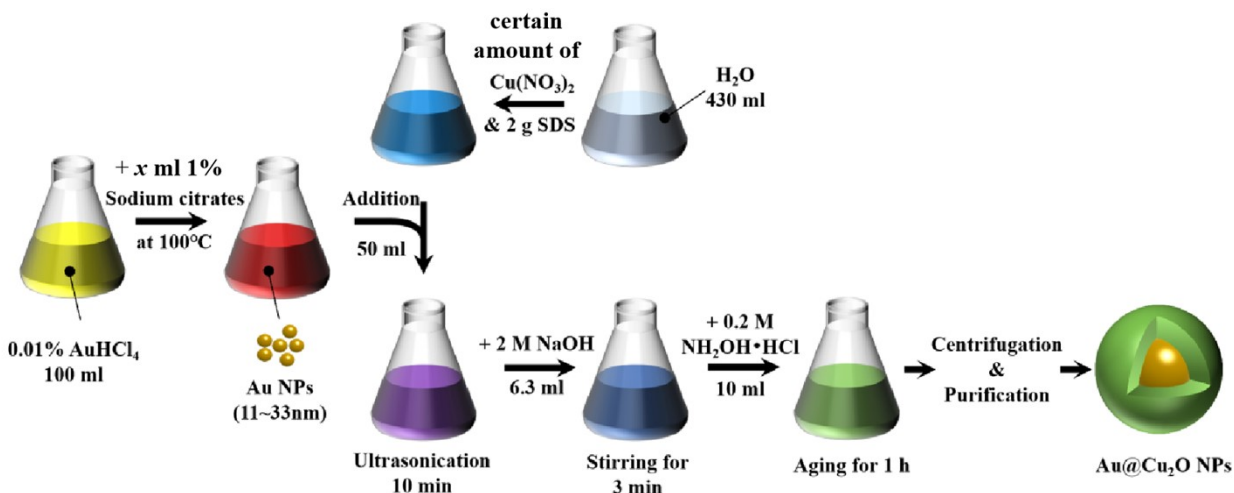
Scheme S1. Schematic illustration of the synthesis of Au@Cu$_2$O core–shell NPs. Here '***x***' equals 0.8, 1.2, 1.8, 2.4 and 3.0 ml. The colors shown are the approximate solution colors observed during the reaction of the synthesis of Au@Cu$_2$O core shell NPs.

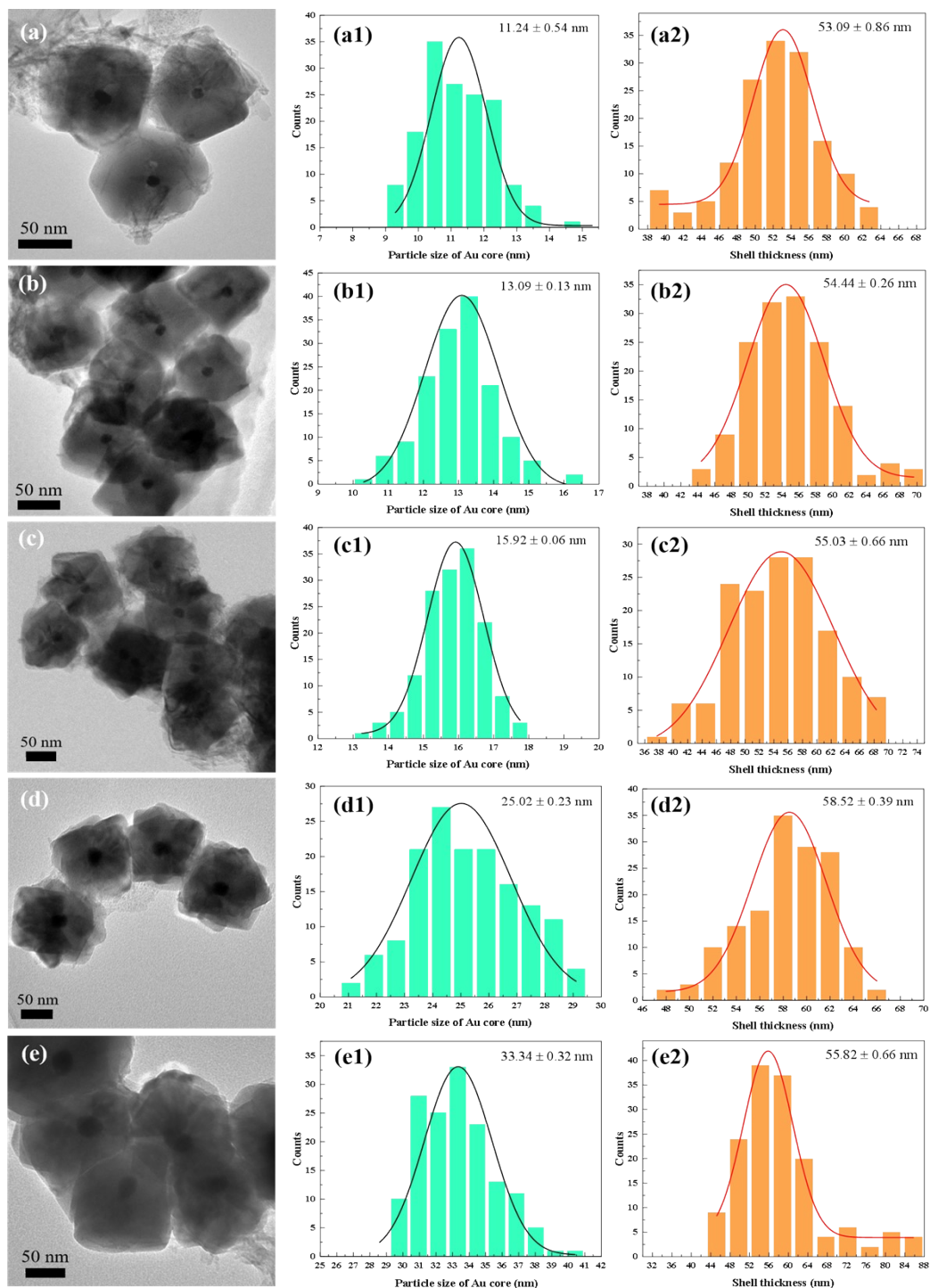## 2. Experimental supplementary data section

Figure S1. TEM images of as-synthesized Au@Cu$_2$O core-shell NPs named (a) 11Au@Cu$_2$O, (b) 13Au@Cu$_2$O, (c) 16Au@Cu$_2$O, (d) 25Au@Cu$_2$O and (e) 33Au@Cu$_2$O. Histograms of (a1 - e1) Au core size and (a2 - e2) Cu$_2$O shell thickness shown in panels a − e, respectively.
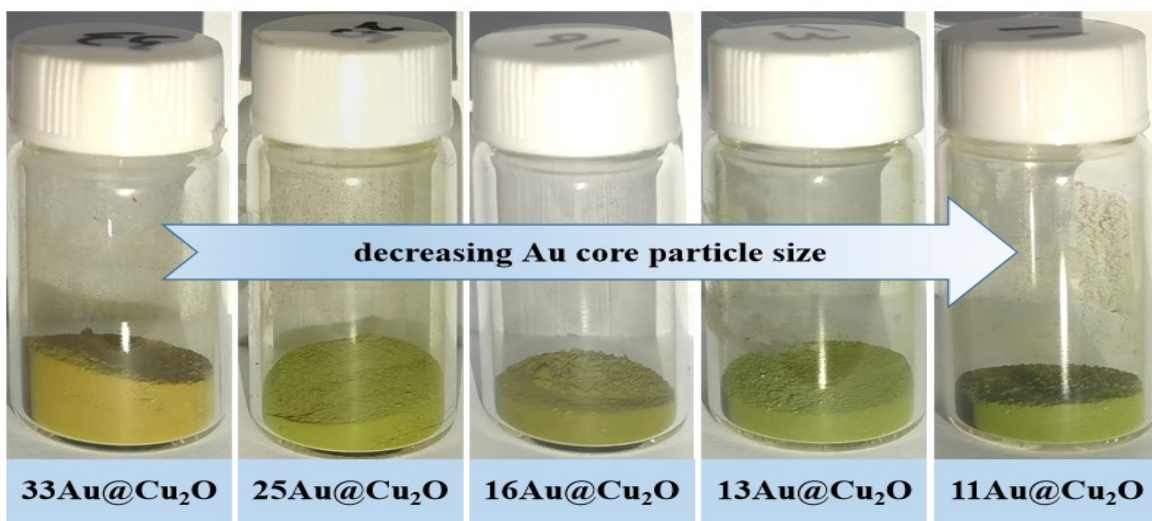
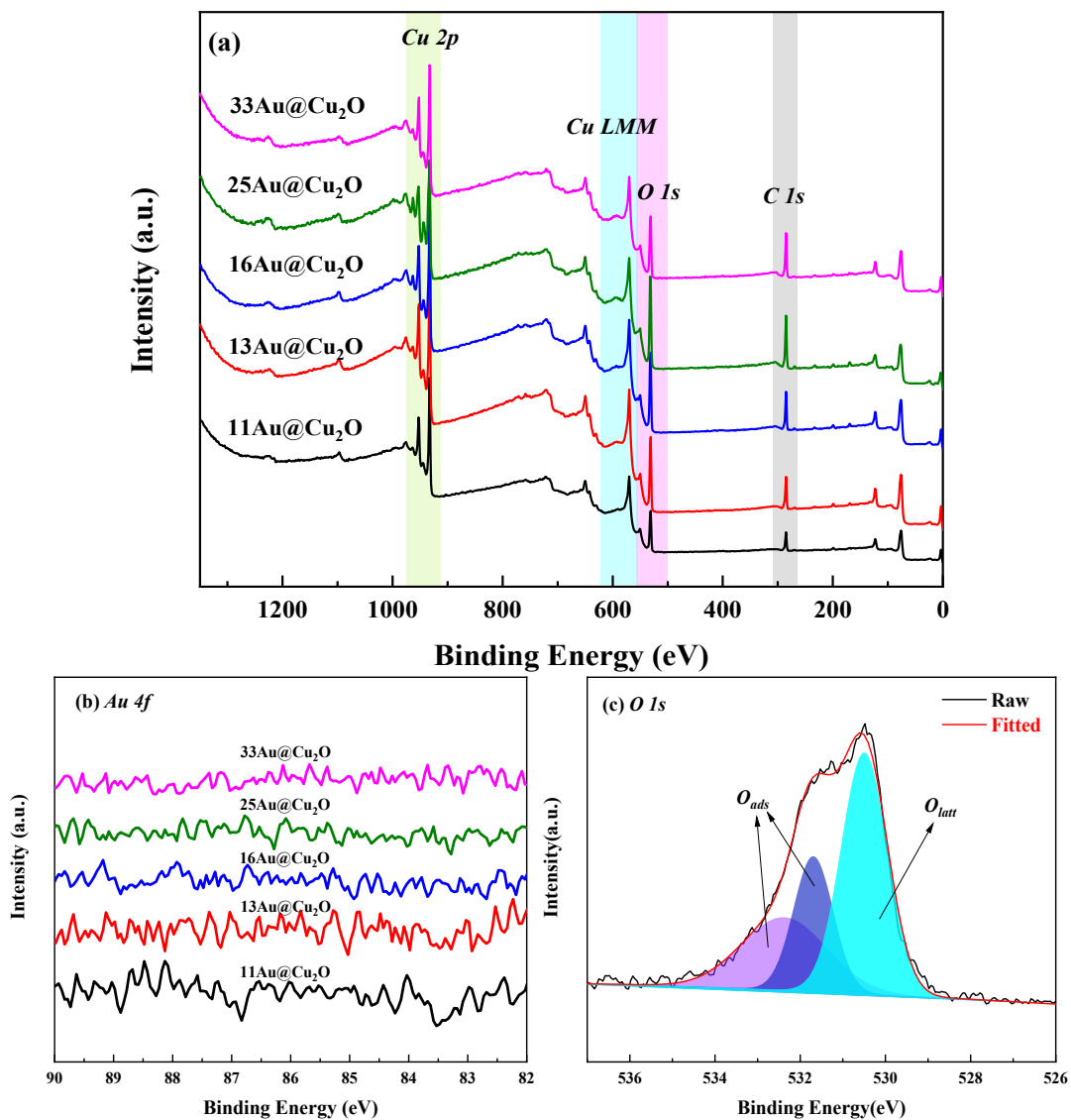**Figure S2.** The color of Au@Cu₂O NPs varies with Au core particle size.

Figure S3. (a) The XPS survey spectrum and (b) High-resolution Au *4f* XPS spectra for Au@Cu$_2$O. (c) High-resolution O *1s* XPS spectra for 16Au@Cu$_2$O.
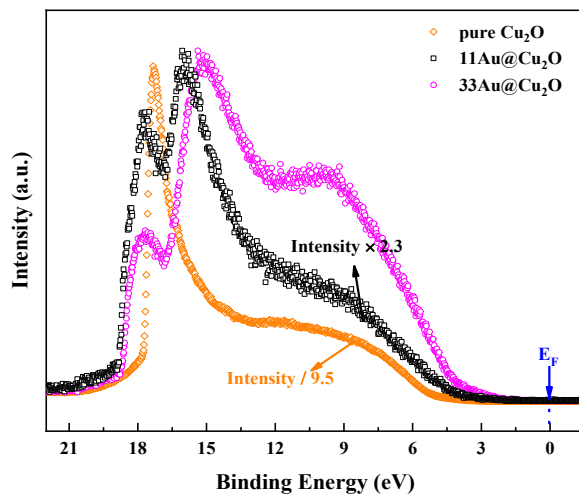
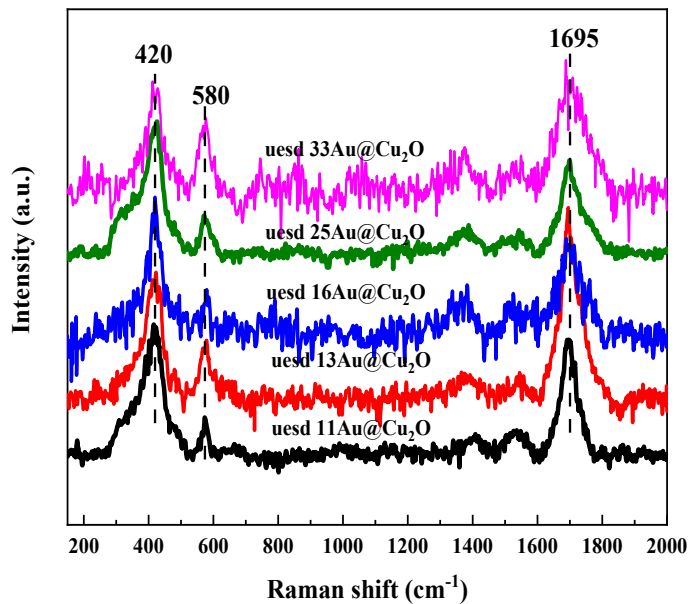**Figure S4.** UPS spectra recorded on pure Cu_2O, $11Au@Cu_2O$ and $33Au@Cu_2O$.
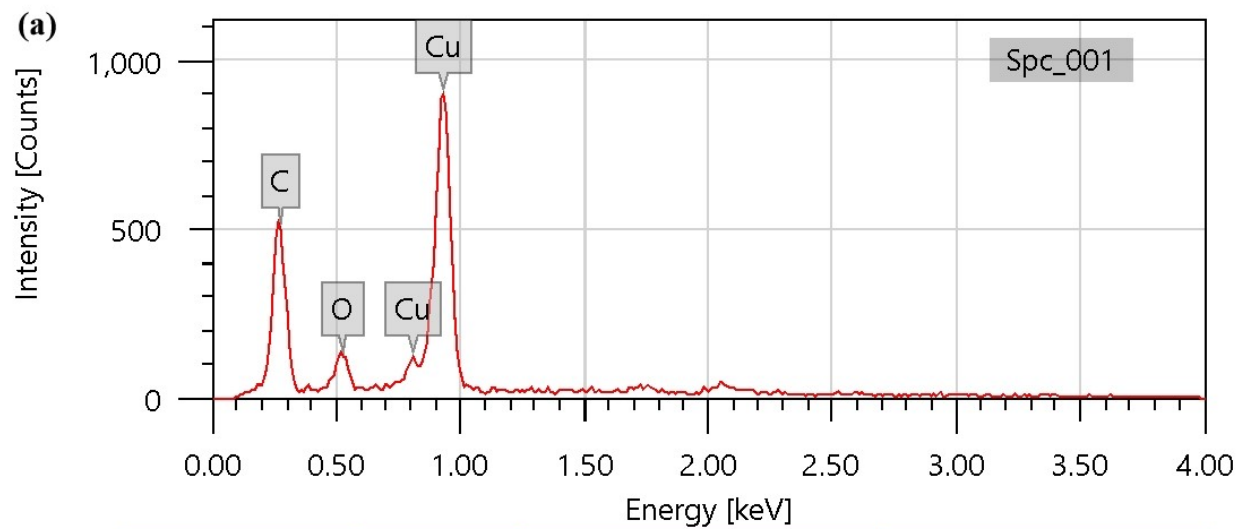

Figure S5. Raman spectra of $Au@Cu_2O$ catalysts after the ethynylation of formaldehyde.

(a)

(b)

Element	Line	Atomic %	Net Error %
C	K	54.62	0.45
O	K	9.95	0.33
Cu	L	35.44	0.47
Au	L	not detected	not detected

Figure S6. (a) The particle EDX-SEM image of 16Au@Cu$_2$O after the ethynylation of formaldehyde. (b) Surface analysis of EDX for 16Au@Cu$_2$O after the ethynylation of formaldehyde.
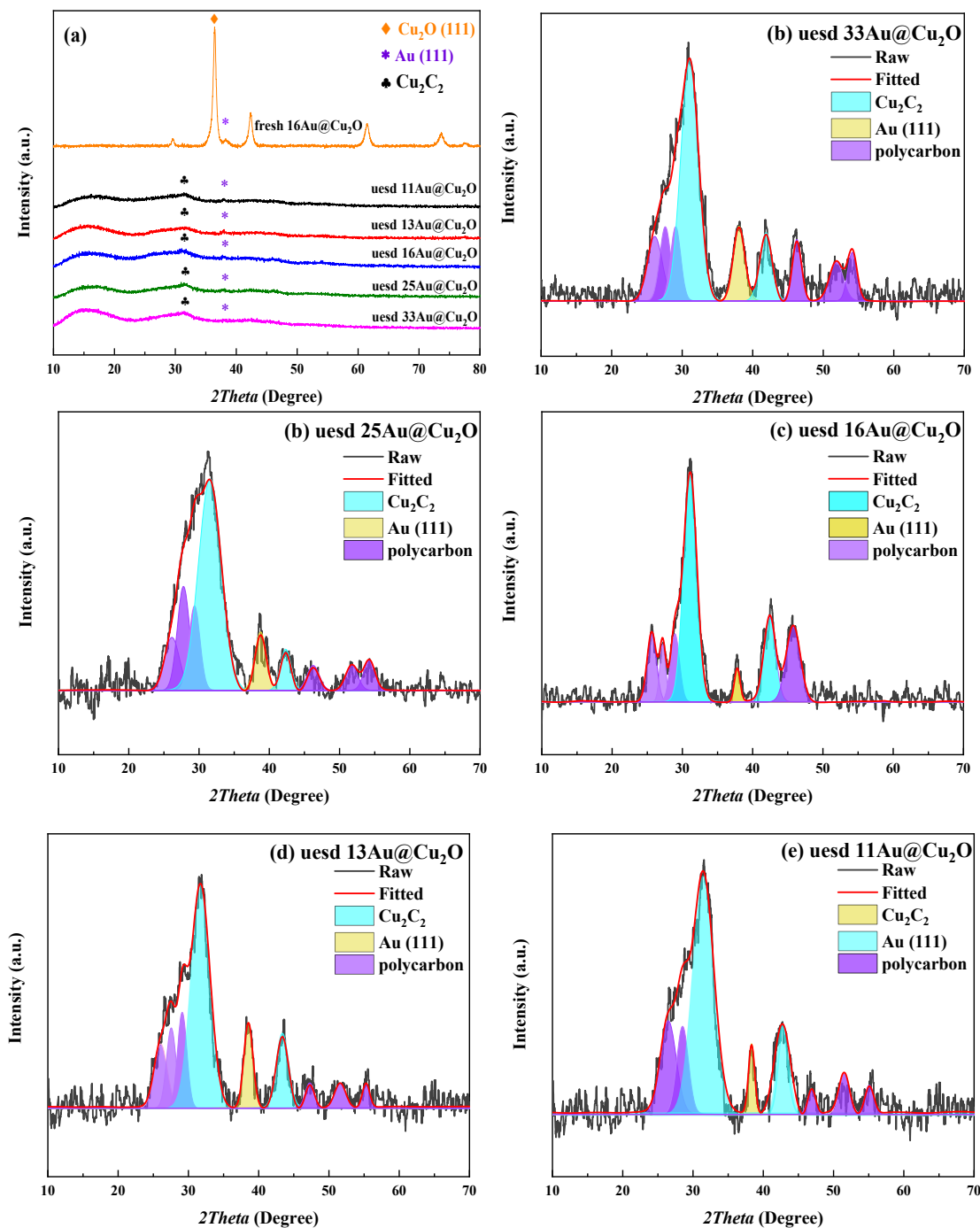
Figure S7. (a) XRD patterns of Au@Cu₂O catalysts after the ethynylation of formaldehyde. (b - f) The enlarged XRD patterns after baseline-correcting and smoothing (15 pts PF smooth) by Origin 2021b software.
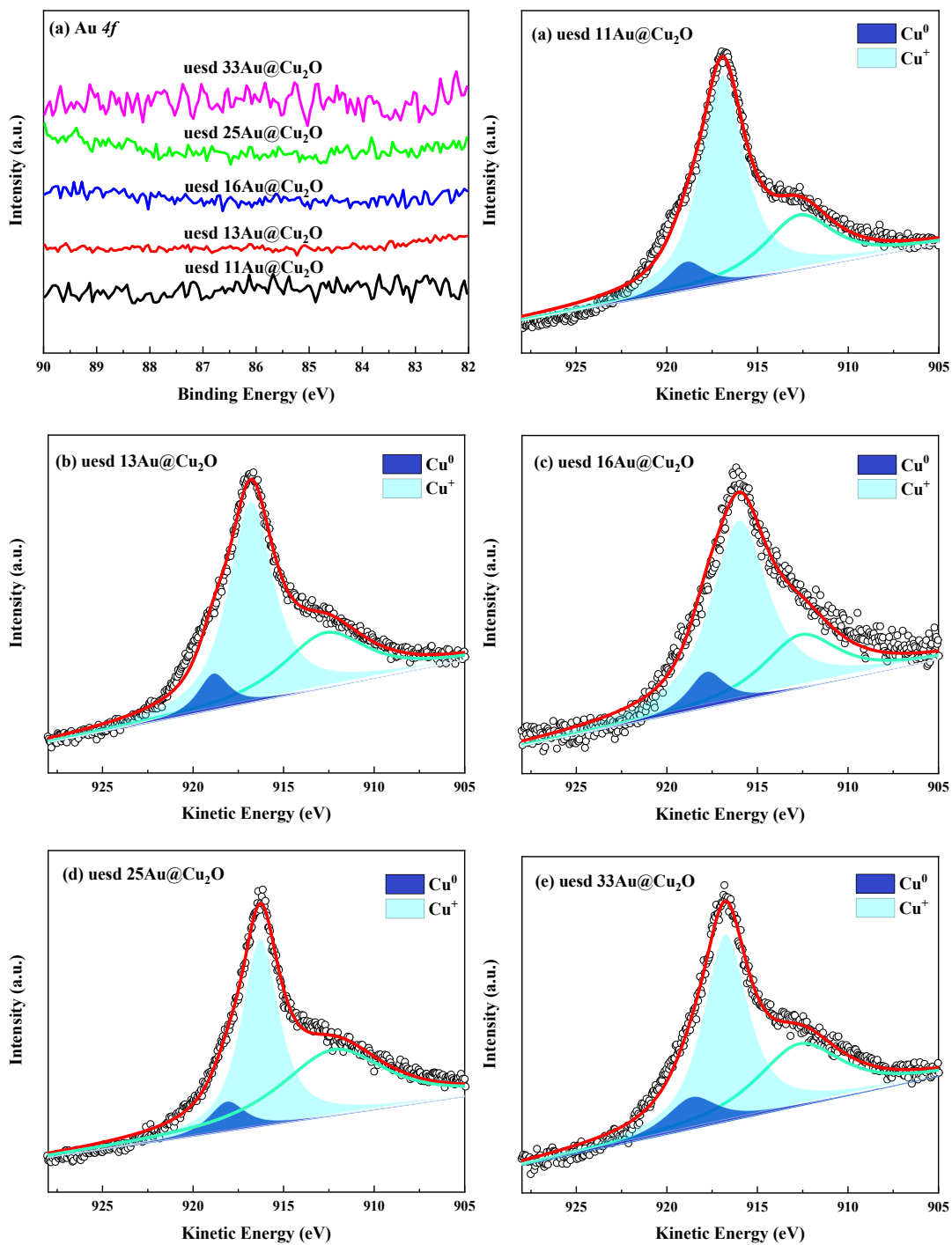
Figure S8. (a) Au 4f XPS spectra and (b - f) Cu LMM Auger spectra of the catalysts after the ethynylation of formaldehyde.

Table S1. Chemical composition, physicochemical properties and catalytic performance of propargyl alcohol in Au@Cu$_2$O samples with different core size.

Sample	Weight ratio (*wt*%)[a]		n_{Cu} ($\times 10^{-2}$ mol·g^{-1})	BET surface area (m^2·g^{-1})[b]	Average pore size (nm)[c]	Catalytic performance[d]	
	Cu	Au				propargyl alcohol yield (%)	propargyl alcohol selectivity (%)
11Au@Cu$_2$O	67.78	1.95	1.07	40.62	22.3	1.37	2.06
13Au@Cu$_2$O	68.76	2.02	1.08	46.77	21.5	1.32	2.01
16Au@Cu$_2$O	72.16	2.12	1.14	55.87	23.9	1.68	2.46
25Au@Cu$_2$O	74.41	2.14	1.17	57.44	19.9	0.96	2.19
33Au@Cu$_2$O	76.93	2.31	1.21	57.41	22.8	0.93	2.32

[a] Cu and Au Content analyzed by ICP-OES. [b] Calculated by the DFT model from the adsorption branches of the isotherms. [c] Calculated by the multipoint BET model from the adsorption date. [d] Reaction conditions: the catalyst (0.25g) was dispersed in 35*wt.*% formaldehyde solution (5ml), and reacted at 90°C for10 h with the C$_2$H$_2$ flow rate of 30 ml/min.

Table S2. Peak position of Cu species, chemical shift ΔE_k, molar ratio of $Cu^+/(Cu^0+Cu^+)$ on the different used catalysts surfaces, and proportion of Cu_2C_2 to Carbyne in different used catalysts[a].

Catalyst	Core size (nm)	Surface information				Bulk information	Ref.
		Peak position[b](eV)		ΔE_k[c] (eV)	$Cu^+/(Cu^0+Cu^+)$[b] (%)	Cu_2C_2/polycarbon[d]	
		Cu^+	Cu^0				
pure Cu_2O	--	916.8	918.6	--	67.6	1.19:1	[1]
Au@Cu_2O	33	916.5	918.3	-0.3	83.9	1.29:1	this work
	25	916.4	918.2	-0.4	85.8	1.40:1	
	16	916.2	918.0	-0.6	88.4	1.60:1	
	13	916.1	917.9	-0.7	88.7	1.64:1	
	11	916.1	917.9	-0.7	89.1	1.66:1	

[a] Reaction conditions: the catalyst (0.25g) was dispersed in 35 *wt.%* formaldehyde solution (5ml), and reacted at 90°C for 10 h with the C_2H_2 flow rate of 30 ml/min. [b] Peak position of Cu species and molar ratio of Cu^+ to Cu^0+Cu^+ were obtained from Figure S8. [c] The XAES chemical shift of Cu^+ for the used catalyst is represented by ΔE_k, $\Delta E_k = E_k(Au@Cu_2O)-E_k(pure\ Cu_2O)$. [d] Proportion of Cu_2C_2 to polycarbon was obtained from Figure S7.

Table S3. Specific fitting function equations and model parameters.

Model	Equation	Equation parameters				
		A_1	A_2	x_0	dx	R^2
$Cu^+/(Cu^0+Cu^+)$ $VS.\Delta E_b$		0.28	0.08	26.03	3.87	1
$Cu_2C_2/polycarbon$ $VS.\Delta E_b$		0.41	0.08	22.26	4.45	1
$Cu^+/(Cu^0+Cu^+)$ $VS.$ Au core size	Boltzmann $\quad y = A_2 + \dfrac{A_1 - A_2}{1 + \exp[(x\text{-}x_0)/dx]}$	89.5	83.07	23.49	4.97	0.9998
$Cu_2C_2/polycarbon$ $VS.$ Au core size		1.70	1.26	21.69	4.55	1
TOF $VS.$ Au core size		0.73	0.39	21.85	1.87	1

References

[1] X. Huang, H. Li, Y. Zhang, R. Wu, L. Ban, L. Xi, Z. Yin, J. Peng, Y. Zhao and L. Fang, *Nanoscale*, 2022, **14**, 13248–13260.